Research Square

Preprints are preliminary reports that have not undergone peer review.
They should not be considered conclusive, used to inform clinical practice,
or referenced by the media as validated information.

Monitoring of Brown Adipose Tissue with β3-Adrenergic Receptor Agonist Using [^{18}F]FDG PET/CT and [^{123}I]mIBG SPECT/CT

Yiseul Choi
Korea Institute of Radiological and Medical Sciences
Eun Sang Lee
Korea Institute of Radiological and Medical Sciences
Jang Woo Park
Korea Institute of Radiological and Medical Sciences
Jin Young Baik
Korea Institute of Radiological and Medical Sciences
Hye Kyung Chung
RayMed., Co., Ltd.
Joo Hyun Kang
kang2325@seoultech.ac.kr

Seoul National University of Science and Technology

Article

Keywords: brown adipose tissue, β3-adrenergic receptor agonist, CL316,243, [18F]FDG PET/CT, [123I]mIBG SPECT/CT, UCP1

Posted Date: September 15th, 2026

DOI: https://doi.org/10.21203/rs.3.rs-10889202/v1

License: This work is licensed under a Creative Commons Attribution 4.0 International License.
Read Full License

Additional Declarations: No competing interests reported.

Version of Record: A version of this preprint was published at Scientific Reports on October 27th, 2026. See the published version at https://doi.org/10.1038/s41598-026-77299-7.

Abstract

Brown adipose tissue (BAT) is a thermogenic organ regulated by sympathetic nervous activation via β3-adrenergic receptors (β3-AR) and serves as a target for metabolic imaging. This study evaluated BAT activation induced by the selective β3-AR agonist CL316,243 using [^{18}F]FDG PET/CT and [^{123}I]mIBG SPECT/CT in male BALB/c mice. Following daily intraperitoneal treatment with CL316,243, uptake of two tracers in interscapular BAT was quantified using volume-of-interest analysis and ex vivo biodistribution. Uncoupling protein 1 (UCP1) expression in BAT was measured by Western blot. Both [^{18}F]FDG PET/CT and [^{123}I]mIBG SPECT/CT successfully monitored CL316,243 induced BAT activation. [^{18}F]FDG PET/CT demonstrated visually conspicuous and quantitatively higher CL316,243-induced uptake differences compared with [^{123}I]mIBG SPECT/CT. Conversely, *ex vivo* biodistribution revealed a higher relative fold increase in [^{123}I]mIBG uptake in interscapular BAT than in [^{18}F]FDG uptake following treatment. White adipose tissue also showed increased uptake of two tracers with CL316,243 treatment. Western blot confirmed elevated UCP1 expression in BAT after CL316,243 treatment. These findings indicate that [^{18}F]FDG PET/CT provides higher sensitivity for *in vivo* visualization of metabolic activation, whereas [^{123}I]mIBG SPECT/CT captures sympathetic tissue responses, demonstrating complementary roles for both tracers in evaluating BAT biology.

Introduction

Brown adipose tissue (BAT) is a specialized thermogenic organ that dissipates chemical energy as heat through mitochondrial uncoupling mediated by uncoupling protein 1 (UCP1)[1–6]. In contrast to white adipose tissue (WAT), BAT is densely vascularized, rich in mitochondria, and extensively innervated by the sympathetic nervous system.[1,5,7] BAT has garnered renewed scientific interest following the identification of metabolically active BAT depots in adult humans through molecular imaging, particularly 2-deoxy-2-[^{18}F]fluoro-D-glucose ([^{18}F]FDG) PET/CT.[8–10] Since this rediscovery, BAT has been increasingly recognized as a relevant modulator of systemic glucose and lipid metabolism and a potential therapeutic target in obesity and metabolic disease.[11–21]

BAT activation is driven primarily by sympathetic stimulation. Norepinephrine released from sympathetic nerve terminals activates β3-adrenergic receptors on brown adipocytes, initiating signaling cascades that enhance lipolysis, mitochondrial respiration, and UCP1 mediated thermogenesis.[4,11,22–28] β3-adrenergic stimulation can also recruit beige or brite adipocytes within WAT, thereby promoting adipose tissue browning.[11–13,26,29–32] Among pharmacologic agents used in experimental BAT studies, CL316,243 is a well-established selective β3-AR agonist with potent effects on BAT activation and WAT browning in rodents.[22,24–26]

[^{18}F]FDG PET/CT is the most widely employed molecular imaging modality for BAT assessment because activated BAT exhibits markedly increased glucose uptake.[8,9,33–34] However, [^{18}F]FDG uptake reflects downstream metabolic demand rather than sympathetic neuronal activity itself.[18,33,34] Consequently,

relying solely on metabolic tracers like [^{18}F]FDG may provide an incomplete picture of the neuro-metabolic coupling that characterizes functional BAT activation. In contrast, ^{123}I-metaiodobenzylguanidine ([^{123}I]mIBG), a norepinephrine analog, is taken up via the norepinephrine transporter and stored in sympathetic nerve terminals, making it a plausible marker of sympathetic innervation and BAT activation.[35,36] Previous research demonstrated that radioiodinated MIBG can visualize BAT and may provide biologically distinct information from that obtained with [^{18}F]FDG.[35] Nevertheless, direct comparative studies between [^{18}F]FDG PET and [^{123}I]mIBG SPECT in β3-adrenergically stimulated BAT remain limited. To achieve a holistic understanding of BAT's physiological state, it is imperative to distinguish between the metabolic response and the sympathetic drive, a distinction that has yet to be systematically evaluated using dual-modality molecular imaging.

In this study, we aim to delineate the complementary roles of [^{18}F]FDG PET/CT and [^{123}I]mIBG SPECT/CT in characterizing the multifaceted nature of BAT activation, thereby establishing a more robust imaging framework for assessing β3-adrenergic-mediated thermogenesis.

Results

CL316,243 treatment markedly increased [^{18}F]FDG uptake in BAT

To assess CL316,243 induced BAT activation, small animal PET/CT imaging was performed in control and CL316,243 treated mice (Fig. 1). Images were acquired at 1 h following [^{18}F]FDG injection. [^{18}F]FDG uptake in BAT was substantially enhanced following CL316,243 treatment. In group analysis, SUV in BAT increased from 0.786 in controls to 9.308 in CL316,243 treated animals. These differences were statistically significant ($p < 0.001$). These findings are consistent with the established increase in glucose utilization in activated BAT following adrenergic stimulation.[33–34,38]

CL316,243 treatment significantly increased [I]mIBG uptake on BAT

To determine whether increased [^{123}I]mIBG uptake could detect BAT activation following β3-adrenergic stimulation in the CL316,243 treated group, mice were intravenously injected with [^{123}I]mIBG. As shown in Fig. 2, [^{123}I]mIBG SPECT/CT imaging revealed a significant treatment effect in interscapular BAT. [^{123}I]mIBG uptake in BAT increased from 0.673 SUV in controls to 2.145 SUV in the CL316,243 treated group; this difference was statistically significant ($p < 0.001$). These data indicate that [^{123}I]mIBG uptake also detected BAT activation following CL316,243 treatment. However, the treatment related differences observed on *in vivo* imaging were less pronounced than those seen with [^{18}F]FDG.

Ex vivo biodistribution confirmed marked BAT activation after CL316,243 treatment

The aforementioned results demonstrated that uptake of both [^{18}F]FDG and [^{123}I]mIBG in BAT was increased by CL316,243 treatment and could be monitored by small animal PET/CT and SPECT/CT, respectively. Therefore, rather than focusing on the superiority of one tracer over the other, we sought to determine whether [^{18}F]FDG and [^{123}I]mIBG capture distinct biological aspects of BAT activation.

Ex vivo biodistribution findings closely paralleled the imaging data in confirming BAT activation; however, the relative fold changes differed from the in vivo imaging results. [^{18}F]FDG uptake in interscapular BAT following CL316,243 treatment increased from 5.52 ± 1.80 to 24.31 ± 10.03%ID/g, corresponding to a 4.4-fold increase ($p = 0.003$) (Fig. 3A, B). [^{18}F]FDG uptake in inguinal WAT increased from 1.63 ± 0.50 to 5.66 ± 2.36%ID/g, corresponding to a 3.5-fold increase ($p = 0.006$).

[^{123}I]mIBG uptake in interscapular BAT following CL316,243 treatment increased from 1.01 ± 0.35%ID/g in control mice to 14.21 ± 3.70%ID/g in CL316,243 treated mice, corresponding to a 14.08-fold increase ($p < 0.001$) (Fig. 3C, D). [^{123}I]mIBG uptake in inguinal WAT increased from 0.53 ± 0.13 to 3.32 ± 0.53%ID/g, corresponding to a 6.2-fold increase ($p < 0.001$).

Although [^{18}F]FDG PET/CT demonstrated more pronounced treatment-related changes on *in vivo* imaging, [^{123}I]mIBG exhibited a greater relative increase in BAT uptake on *ex vivo* biodistribution. This discrepancy suggests that the two radiotracers reflect distinct aspects of BAT activation rather than indicating the superiority of one over the other.

Western blot analysis demonstrated increased UCP1 expression in BAT

To determine whether BAT activation was associated with increased UCP1 protein expression, we evaluated UCP1 levels in interscapular BAT by Western blot (Fig. 4). UCP1 expression was significantly increased in the CL316,243 treated group compared with the control group ($p = 0.001$), using COX4 as the loading control. This increase in UCP1 is biologically consistent with enhanced thermogenic activation and supports the interpretation of the *in vivo* imaging and *ex vivo* biodistribution findings.[2–4,27,28,31,32,39] Accordingly, the increased tracer uptake observed *in vivo* was accompanied by molecular evidence of BAT activation.

Discussion

This study demonstrated that both [^{18}F]FDG PET/CT and [^{123}I]mIBG SPECT/CT can monitor BAT activation induced by CL316,243 as β3-adrenergic receptor agonist. The major findings were as follows. First, CL316,243 significantly increased interscapular BAT uptake of both [^{18}F]FDG and [^{123}I]mIBG in mice. Second, [^{18}F]FDG PET/CT showed a more visually prominent and quantitatively larger treatment-related change than [^{123}I]mIBG SPECT/CT. Third, *ex vivo* biodistribution demonstrated a larger fold

increase in [^{123}I]mIBG uptake in BAT than that in [^{18}F]FDG. Fourth, the enhanced UCP1 expression after CL316,243 treatment validated that the uptake changes of two tracers reflected thermogenic activation.

The strong treatment effect observed with [^{18}F]FDG PET/CT is consistent with the established role of [^{18}F]FDG as a marker of activated BAT metabolism.[8,9,33–34,38] Activated BAT displays increased glucose transport and glycolytic activity, particularly under sympathetic or pharmacologic stimulation, and [^{18}F]FDG has therefore become the most widely used imaging biomarker of BAT activity.[8,9,18,33] Our results align with previous rodent studies showing that β3-adrenergic stimulation enhances [^{18}F]FDG accumulation in BAT and can also increase uptake in browning WAT.[22,26,38] In the present dataset, the differences between control and CL316,243 treated animals was especially evident on [^{18}F]FDG PET/CT, both visually and quantitatively, indicating that [^{18}F]FDG was highly sensitive for in vivo detection of treatment-induced BAT activation. [^{123}I]mIBG SPECT/CT also detected a significant treatment effect, but the imaging contrast was less dramatic than that observed with [^{18}F]FDG PET/CT. This observation is noteworthy because the present data do not support a simple claim that [^{18}F]FDG is superior to [^{123}I]mIBG for BAT imaging. Rather, the relative performance of the two radiotracers depends on the mode of assessment. The more striking in vivo performance of [^{18}F]FDG is biologically plausible because BAT activation is accompanied by a marked increase in glucose utilization, and technically plausible because PET generally provides higher sensitivity and spatial resolution than SPECT. Accordingly, [^{18}F]FDG PET/CT appears more effective for visualizing treatment-induced BAT activation under the imaging conditions used in this study. At the same time, *ex vivo* biodistribution revealed a different pattern. *Ex vivo* biodistribution demonstrated a 14.08-fold increase in [^{123}I]mIBG accumulation in interscapular BAT after CL316,243 treatment, whereas the corresponding increase for [^{18}F]FDG was 4.40-fold. This discrepancy between in vivo imaging and *ex vivo* biodistribution suggests that the two radiotracers reflect different aspects of BAT biology rather than one tracer being uniformly superior. [^{18}F]FDG primarily represents increased glucose metabolism in activated BAT, whereas [^{123}I]mIBG likely reflects sympathetic nerve terminal function, norepinephrine transporter-mediated uptake, and catecholamine storage capacity.[35] Thus, relatively large increase in [^{123}I]mIBG uptake in BAT by *ex vivo* biodistribution may indicate a strong adrenergic or sympathetic tissue response that was less dramatically visualized on [^{123}I]mIBG SPECT/CT than the metabolic response on [^{18}F]FDG PET/CT.

The divergent patterns between imaging and *ex vivo* biodistribution may also be influenced by methodological factors. Small animal PET typically provides better spatial resolution and signal sensitivity than small animal SPECT, which can affect visualization of relatively small BAT in size. Image-derived VOIs measurements are also subject to partial-volume effects, reconstruction parameters, attenuation and scatter correction differences, and display window settings. In contrast, biodistribution directly measures tissue radioactivity *ex vivo* and is not limited by image resolution. Therefore, the stronger visual and VOIs-based treatment contrast on [^{18}F]FDG PET/CT and the larger fold change on [^{123}I]mIBG biodistribution are not necessarily contradictory; rather, they likely reflect the different biological targets and technical characteristics of the two approaches.

Furthermore, CL316,243 treatment increased tracer uptake in both classical BAT and inguinal WAT, consistent with the established ability of β3-adrenergic agonists to induce WAT browning.[11–13,25,28–31] However, the relative treatment effect was stronger in BAT than in WAT for both radiotracers. The CL316,243 treatment to control fold change for [^{123}I]mIBG uptake was 14.08 in interscapular BAT versus 6.24 in inguinal WAT. For [^{18}F]FDG, the corresponding ratios were 4.40 and 3.48. This pattern supports the interpretation that CL316,243 treatment induced a stronger response in classical BAT than in inguinal WAT, although both BAT and WAT were responsive to β3-adrenergic stimulation.

The Western blot findings further strengthened the biological validity of the imaging data. UCP1 is the standard molecular marker of thermogenic adipocytes and is essential for canonical BAT heat production.[2–4,31,39] Increased UCP1 expression after CL316,243 treatment confirms that the observed radiotracer uptake changes were associated with true thermogenic activation rather than nonspecific perfusion changes or radiotracer redistribution. The concordance among imaging, *ex vivo* biodistribution, and tissue protein analysis is therefore a major strength of the present study.

From a translational perspective, the present findings suggest complementary roles for [^{18}F]FDG and [^{123}I]mIBG in BAT imaging. [^{18}F]FDG PET/CT appears highly effective for in vivo visualization of metabolically activated BAT, whereas [^{123}I]mIBG may provide additional information related to sympathetic BAT activation that is not fully captured by [^{18}F]FDG alone. Human studies showing BAT recruitment with cold exposure or β3-adrenergic agonists further support the relevance of this framework.[20,21] Although direct translation from mouse models to human BAT imaging should be interpreted cautiously, the current results suggest that multimodal imaging may improve mechanistic assessment of BAT responses.

This study has several limitations. The study focused mainly on interscapular BAT, which is an ideal tissue in mice but does not fully recapitulate the more heterogeneous BAT distribution in humans.[16,17] In addition, formal kinetic analysis was not performed, and the quantitative relationship between image-based uptake and tissue-based biodistribution was not modeled mathematically. Nonetheless, the internal consistency of the overall dataset supports the reliability of the central conclusions. Taken together, the present results indicate that [^{18}F]FDG and [^{123}I]mIBG should not be ranked in simple terms of superiority. Instead, they appear to serve different but complementary functions. [^{18}F]FDG PET/CT is more sensitive for in vivo visualization of CL316,243 treatment-induced BAT metabolic activation under the present conditions, whereas [^{123}I]mIBG may better highlight the relative magnitude of sympathetic BAT response at the tissue level. This complementary interpretation more accurately reflects the experimental findings.

Conclusion

CL316,243 induced β3-adrenergic stimulation significantly increased the uptake of [^{18}F]FDG and [^{123}I]mIBG in murine BAT. In this study, [^{18}F]FDG PET/CT showed a more prominent treatment-related

change in BAT than [^{123}I]mIBG SPECT/CT, indicating high sensitivity for *in vivo* monitoring the metabolic activation in BAT. In contrast, [^{123}I]mIBG uptake in BAT demonstrated a larger fold increase in *ex vivo* biodistribution after CL316,243 treatment, suggesting that it may reflect a distinct aspect of adrenergic or sympathetic BAT activation. Together, these findings indicate that [^{18}F]FDG and [^{123}I]mIBG provide complementary information for evaluating BAT activation rather than supporting the unequivocal superiority of one radiotracer over the other.

Methods

Animals and CL316,243 treatment

All experimental procedures were performed in accordance with the relevant guidelines and regulations and were approved by the Institutional Animal Care and Use Committee (IACUC) of KIRAMS (kirams 2024-0022). Male BALB/cAnNTac mice, mice under specific pathogen-free conditions were purchased from DBL Inc. (Korea) and underwent a one-week acclimation period. Approximately 6-week-old mice were used in this study. Animals were housed under standard laboratory conditions with free access to water and standard chows except during fasting before imaging. CL316,243 (1 mg/kg) or saline was administered intraperitoneally to the mice every morning for 7 days.

Mice were fasted for overnight before acquiring small-animal PET/CT or SPECT/CT imaging. [^{18}F]FDG and [^{123}I]mIBG were synthesized at the Korea Institute of Radiological and Medical Sciences using a cyclotron facility in accordance with previously described methods.[36,37] [^{18}F]FDG or [^{123}I]mIBG was intravenously injected into mice under anesthesia with a 2.5–3.0% isoflurane in O_2, and tracer uptake was carried out for 1 h in a dark environment while the animals remained anesthetized. The animals were euthanized by CO_2 inhalation at the end of the experiments.

Small animal PET/CT image acquisition and quantitative analysis

Small animal PET/CT imaging was performed using a Nano-Scan PET/CT system (Mediso, Budapest, Hungary). A dedicated multi mouse imaging bed (4-mice bed, Mediso) was used to enable simultaneous acquisition of up to four mice under identical imaging conditions. Mice were divided into groups of four animals, anesthetized with 2.5–3.0% isoflurane in O_2, and intravenously injected with [^{18}F]FDG (4.912 ± 0.255 MBq/200 μL) via the tail vein.

Following tracer administration, animals were maintained under isoflurane anesthesia during the 1 h uptake period. Static PET images were subsequently acquired for 20 min using an energy window of 400–600 keV. CT imaging was performed immediately after PET image acquisition for anatomical reference and attenuation correction using the following parameters: 50 kVp, 100 μA, 170 ms exposure time, and an isotropic voxel size of 0.25 mm.

Image reconstruction was performed after completion of both PET and CT acquisitions using a three-dimensional ordered-subset expectation maximization (3D-OSEM) algorithm with four iterations and six subsets, resulting in a voxel size of 0.4 mm. Corrections for attenuation, scatter, and radioactive decay were applied during reconstruction.

For quantitative analysis, PET images were co-registered with corresponding CT images, and volumes of interest (VOIs) were manually delineated in brown adipose tissue regions. Tracer uptake was quantified as standardized uptake values (SUVs), calculated based on injected dose and body weight. All image processing and quantitative analyses were performed using PMOD software (Version 3.8).

Small animal SPECT/CT image acquisition and quantitative analysis

Small animal SPECT/CT imaging was performed using a Nano-Scan SPECT/CT system (Mediso, Budapest, Hungary). All mice (n = 4 per group) were maintained under anesthesia with 2.5–3.0% isoflurane in O_2 during injection, throughout the 1 h uptake period, and during image acquisition. Mice received an intravenous injection of [^{123}I]mIBG (37.263 ± 1.290 MBq/200 µL) via the tail vein.

SPECT data were acquired using a 256 × 256 matrix, with 20 projections and an acquisition time of 45 s per projection. A 20% energy window centered on the 159 keV photopeak of iodine-123 was applied. CT imaging was performed after SPECT acquisition for attenuation correction and anatomical localization using the following parameters: 50 kVp, 980 µA, and a 300 ms exposure time, and an isotropic voxel size of 25 mm.

Image reconstruction was performed after completion of both SPECT and CT acquisitions using a hybrid algorithm combining ordered-subset expectation maximization (OSEM) and maximum likelihood expectation maximization (MLEM), incorporating Monte Carlo-based corrections, resulting in a voxel size of 0.25 mm.

For quantitative analysis, SPECT images were co-registered with corresponding CT images, and VOIs were delineated in brown adipose tissue regions. Tracer uptake was converted into SUVs using a calibration factor (kBq/cc per image unit). All image processing and quantitative analyses were performed using PMOD software (Version 3.8).

Western blot analysis

BAT samples were lysed in RIPA buffer (Thermo Scientific, Waltham, MA, USA, 89901) supplemented with a Halt™ Protease Inhibitor Cocktail (Thermo Scientific, Waltham, MA, USA, 78439) using a microtube homogenizer (Nippi, Tokyo, Japan, 893131) and subsequently centrifuged at 15,000 × g for 10 min at 4°C. A total of 32 µg of BAT lysate was separated by 15% SDS-polyacrylamide gel electrophoresis (SDS-

PAGE) and transferred to a PVDF membrane for immunoblotting. Membranes were probed with primary antibodies against UCP1 (MAB6158, R&D Systems, Minneapolis, MN, USA) or COX4 (ab14744, Abcam, Cambridge, UK), and signals were visualized using an enhanced chemiluminescence (ECL) detection kit (Bio-Rad). The intensity of UCP1 and COX4 was quantified using ImageJ software.

Ex vivo Biodistribution study

Mice (n = 5 per group) were intravenously administered with either [^{123}I]mIBG (0.797 ± 0.254 MBq) or [^{18}F]FDG (0.815 ± 0.066 MBq). At 1 h post-injection, the animals were anesthetized with 2.5–3.0% isoflurane in O_2, followed by blood collection via cardiac puncture. The animals were then euthanized for biodistribution analysis. A total of 18 tissues, including the heart, interscapular brown fat, inguinal white fat and blood (obtained via cardiac puncture), were harvested and weighed. The radioactivity of each tissue was then measured for 1 min using a gamma counter (PerkinElmer). To ensure quantification accuracy, 1/10 and 1/100 standards of the injected dose were counted simultaneously. The results were normalized to tissue weight and expressed as the percentage of injected dose per gram (% ID/g).

Statistical analysis

A statistically significant difference was determined using a two-tailed Student's *t*-test performed in SPSS version 23.0 (IBM SPSS, USA). A p value < 0.05 was considered statistically significant.

Declarations

Acknowledgement

This work was supported by the National Research Foundation of Korea (NRF, No. RS-2022-00197770) grant and by a grant from the Korea Institute of Radiological and Medical Science (KIRAMS) funded by the Korean government (Ministry of Science and ICT, No.50539-2026).

AuthorContributions

Chung is the co-corresponding author of this article. J.H.K. and H.K.C. conceived and designed the study. Y.C. and E.S.L. performed animal experiments and collected tissue samples. J.Y.B. generated the Western blot data from tissue samples, and J.W.P. analyzed the acquired imaging data. J.H.K., H.K.C., and Y.C. wrote the first draft of the manuscript. All authors read and approved the final manuscript.

Data availability

The data generated and/or analyzed during the current study are available from the corresponding author on reasonable request.

Competing interests

The authors declare no competing financial interests.

Additional Information

Correspondence and requests for materials should be addressed to Kang.

References

1. Cannon, B. & Nedergaard, J. Brown adipose tissue: function and physiological significance. *Physiol. Rev.* **84**, 277–359 (2004).
2. Enerbäck, S. et al. Mice lacking mitochondrial uncoupling protein are cold-sensitive but not obese. *Nature* **387**, 90–94 (1997).
3. Matthias, A. et al. Thermogenic responses in brown fat cells are fully UCP1-dependent. *J. Biol. Chem.* **275**, 25073–25081 (2000).
4. Lowell, B. B. & Spiegelman, B. M. Towards a molecular understanding of adaptive thermogenesis. *Nature* **404**, 652–660 (2000).
5. Himms-Hagen, J. Brown adipose tissue thermogenesis: interdisciplinary studies. *FASEB J.* **4**, 2890–2898 (1990).
6. Smith, R. E. & Horwitz, B. A. Brown fat and thermogenesis. *Physiol. Rev.* **49**, 330–425 (1969).
7. Richard, D. & Picard, F. Brown fat biology and thermogenesis. *Front. Biosci. (Landmark Ed)*. **16**, 1233–1260 (2011).
8. Cypess, A. M. et al. Identification and importance of brown adipose tissue in adult humans. *N Engl. J. Med.* **360**, 1509–1517 (2009).
9. van Lichtenbelt, M. Cold-activated brown adipose tissue in healthy men. *N Engl. J. Med.* **360**, 1500–1508 (2009).
10. Nedergaard, J., Bengtsson, T. & Cannon, B. Unexpected evidence for active brown adipose tissue in adult humans. *Am. J. Physiol. Endocrinol. Metab.* **293**, E444–E452 (2007).
11. Harms, M. & Seale, P. Brown and beige fat: development, function and therapeutic potential. *Nat. Med.* **19**, 1252–1263 (2013).
12. Wu, J. et al. Beige adipocytes are a distinct type of thermogenic fat cell in mouse and human. *Cell* **150**, 366–376 (2012).
13. Seale, P. et al. Transcriptional control of brown fat determination by PRDM16. *Cell. Metab.* **6**, 38–54 (2007).
14. Yoneshiro, T. et al. Age-related decrease in cold-activated brown adipose tissue and accumulation of body fat in healthy humans. *Obes. (Silver Spring)*. **19**, 1755–1760 (2011).
15. Yoneshiro, T., Aita, S., Kawai, Y., Iwanaga, T. & Saito, M. Nonpungent capsaicin analogs activate thermogenesis and increase energy expenditure in humans. *Am. J. Clin. Nutr.* **95**, 845–850 (2012).

16. Lidell, M. E. et al. Evidence for two types of brown adipose tissue in humans. *Nat. Med.* **19**, 631–634 (2013).
17. Betz, M. J. & Enerbäck, S. Human brown adipose tissue: what we have learned so far. *Diabetes* **64**, 2352–2360 (2015).
18. Carpentier, A. C. et al. Brown adipose tissue energy metabolism in humans. *Front. Endocrinol. (Lausanne)*. **9**, 447 (2018).
19. Scheele, C. & Wolfrum, C. Brown adipose crosstalk in tissue plasticity and human metabolism. *Endocr. Rev.* **41**, 53–65 (2020).
20. van der Lans, A. A. J. J. et al. Cold acclimation recruits human brown fat and increases nonshivering thermogenesis. *J. Clin. Invest.* **123**, 3395–3403 (2013).
21. O'Mara, A. E. et al. Chronic mirabegron treatment increases human brown fat, HDL cholesterol, and insulin sensitivity. *J. Clin. Invest.* **130**, 2209–2219 (2020).
22. Himms-Hagen, J. et al. Effect of CL-316,243, a thermogenic β_3-agonist, on energy balance and brown and white adipose tissues in rats. *Am. J. Physiol.* **266**, R1371–R1382 (1994).
23. Collins, S., Daniel, K. W., Rohlfs, E. M., Ramkumar, V. & Taylor, I. L. Impaired expression and functional activity of the β_3- and β_1-adrenergic receptors in adipose tissue of C57BL/6J mice. *Mol. Endocrinol.* **8**, 518–527 (1994).
24. Arch, J. R. S. β_3-Adrenoceptor agonists: potential, pitfalls and progress. *Eur. J. Pharmacol.* **440**, 99–107 (2002).
25. Arch, J. R. S. Challenges in β_3-adrenoceptor agonist drug development. *Ther. Adv. Endocrinol. Metab.* **2**, 59–64 (2011).
26. Ghorbani, M., Claus, T. H. & Himms-Hagen, J. Hypertrophy of brown adipocytes in brown and white adipose tissues and reversal by CL 316,243 treatment. *Am. J. Physiol.* **273**, E444–E452 (1997).
27. Festuccia, W. T., Oztezcan, S., Laplante, M., Berthiaume, M. & Gélinas, Y. Noradrenaline-induced uncoupling protein-1 expression in rat brown adipocytes requires PPARγ and p38 MAPK signaling. *Am. J. Physiol. Regul. Integr. Comp. Physiol.* **285**, R153–R161 (2003).
28. Mottillo, E. P., Bloch, A. E., Leff, T. & Granneman, J. G. Lipolytic products activate peroxisome proliferator-activated receptor α and δ

in brown adipocytes to match fatty acid oxidation with supply. *J. Biol. Chem.* **287**, 25038–25048 (2012).

29. Cousin, B. et al. Occurrence of brown adipocytes in rat white adipose tissue: molecular and morphological characterization. *J. Cell. Sci.* **103**, 931–942 (1992).
30. Frontini, A. et al. White-to-brown transdifferentiation of omental adipocytes in patients affected by pheochromocytoma. *Biochim. Biophys. Acta*. **1831**, 950–959 (2013).
31. Shabalina, I. G. et al. UCP1 in brite/beige adipose tissue mitochondria is functionally thermogenic. *Cell. Rep.* **5**, 1196–1203 (2013).
32. Kajimura, S. et al. Regulation of the brown and white fat gene programs through a PRDM16/CtBP transcriptional complex. *Genes Dev.* **22**, 1397–1409 (2008).
33. Orava, J. et al. Different metabolic responses of human brown adipose tissue to activation by cold and insulin. *Cell. Metab.* **14**, 272–279 (2011).
34. Muzik, O., Diwadkar, V. A., Robinson, G. W., Janisse, J. & Granneman, J. G. Imaging brown adipose tissue function and metabolic activity. *Q. J. Nucl. Med. Mol. Imaging*. **56**, 112–121 (2012).
35. Okuyama, C. et al. ^{123}I- or ^{125}I-metaiodobenzylguanidine visualization of brown adipose tissue. *J. Nucl. Med.* **43**, 1234–1240 (2002).
36. Choi, Y. et al. Feasibility study of single-photon emission computed tomography with Iodine-123 labeled metaiodobenzylguanidine for preclinical evaluation of labetalol as a β-adrenergic receptor blocker. *Mol. Pharm.* **21**, 2435–2440 (2024).
37. Park, I. W. et al. ^{18}F-FDG PET/CT monitoring of β_3 agonist-stimulated brown adipocyte recruitment in white adipose tissue. *J. Nucl. Med.* **56**, 153–158 (2015).
38. Fedorenko, A., Lishko, P. V. & Kirichok, Y. Mechanism of fatty-acid-dependent UCP1 uncoupling in brown fat mitochondria. *Cell* **151**, 400–413 (2012).
39. Kim, S. W. A steady production of [^{18}F]FDG with KIRAMS-13 cyclotron at KIRAMS. *17th International Conference on Cyclotrons and Their* Applications, Tokyo, Japan, 18–22 p. 18. (2004).

Figures

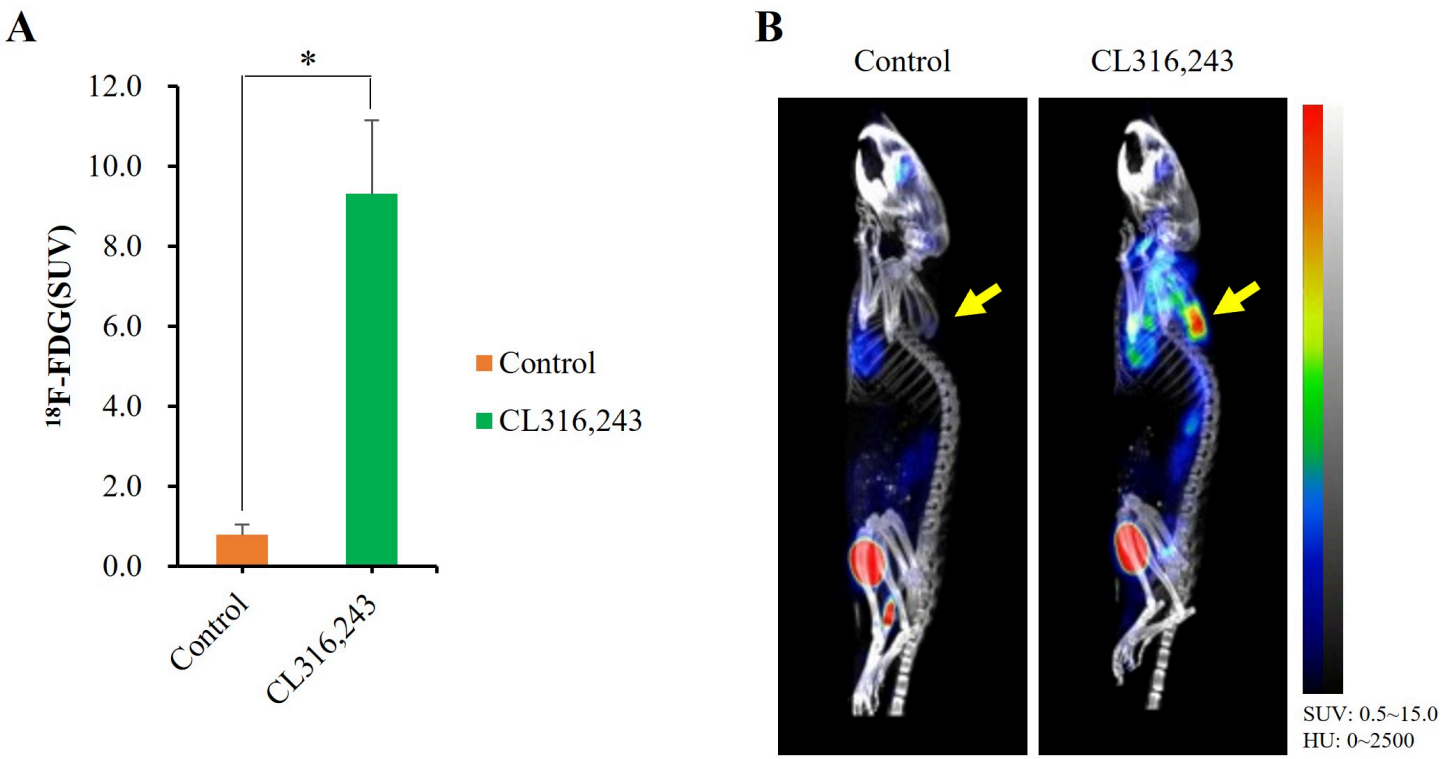


Figure 1

Evaluation of [^{18}F]FDG uptake in interscapular BAT by CL316,243 treatment using small animal PET/CT. (A) Quantitative analysis of PET/CT image for [^{18}F]FDG uptake in each group. [^{18}F]FDG uptake of interscapular BAT was quantified as SUV. * $p < 0.05$, compared to CL316,243 treated group. Data is presented as mean ± SD. (B) Representative MIP images of [^{18}F]FDG PET/CT were obtained 1 h following [^{18}F]FDG injection in control and CL316,243 treated mice. The arrow indicates interscapular BAT.

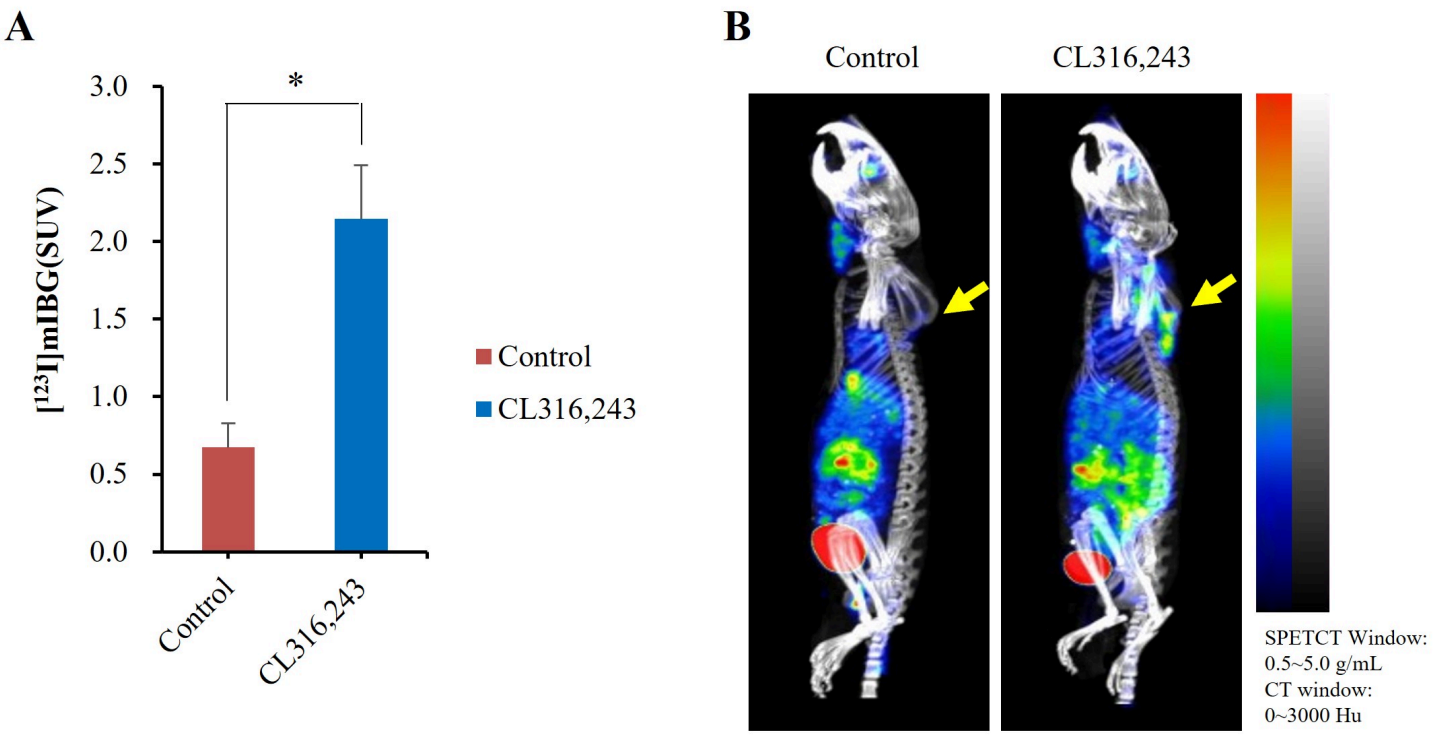
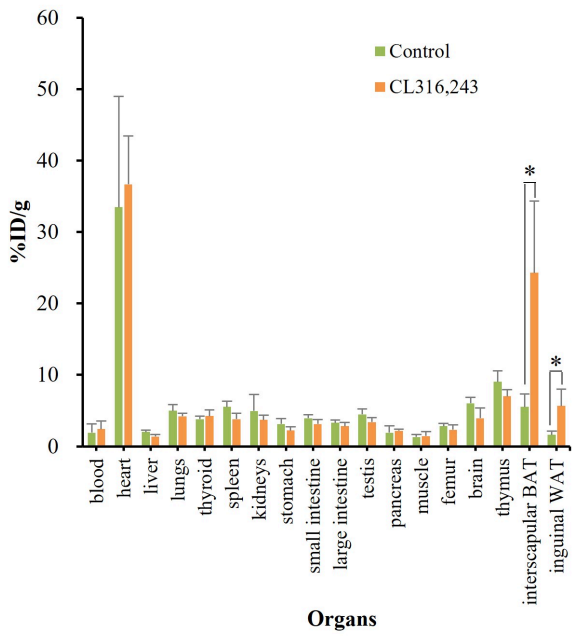


Figure 2

Evaluation of [^{123}I]mIBG uptake in interscapular BAT in CL316,243 treatment using small animal SPECT/CT. (A) Quantitative analysis of SPECT/CT image for [^{123}I]mIBG uptake in each group. [^{123}I]mIBG uptake of interscapular BAT was quantified as SUV. * $p < 0.05$, compared to CL316,243 treated group. Data is presented as mean ± SD. (B) Representative MIP images of [^{123}I]mIBG SPECT/CT were obtained 1 h following [^{123}I]mIBG injection in control and CL316,243 treated mice. The arrow indicates interscapular BAT.

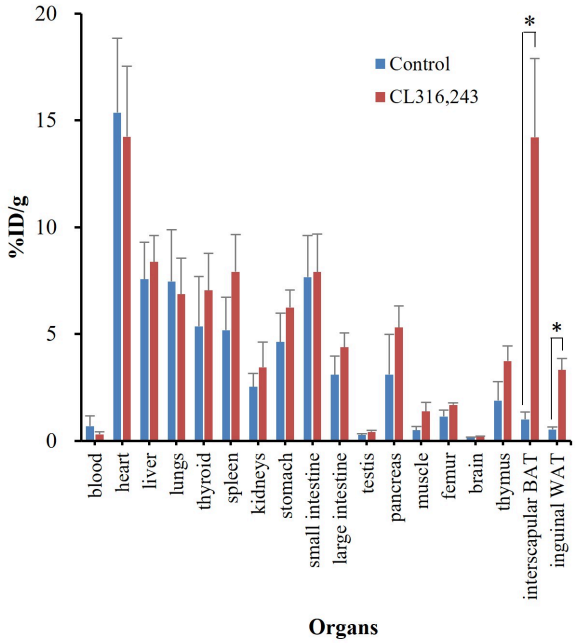
A



B

organs \ group	[18F]FDG %ID/g Control	CL316,243
blood	1.91 ± 1.24	2.42 ± 1.17
heart	33.49 ± 15.54	36.68 ± 6.81
liver	2.01 ± 0.26	1.38 ± 0.28
lungs	4.99 ± 0.89	4.22 ± 0.40
thyroid	3.80 ± 0.47	4.26 ± 0.85
spleen	5.51 ± 0.81	3.79 ± 0.82
kidneys	4.95 ± 2.31	3.70 ± 0.69
stomach	3.14 ± 0.75	2.21 ± 0.56
small intestine	3.94 ± 0.52	3.13 ± 0.62
large intestine	3.31 ± 0.38	2.82 ± 0.56
testis	4.48 ± 0.73	3.39 ± 0.63
pancreas	1.91 ± 0.97	2.18 ± 0.24
muscle	1.30 ± 0.38	1.43 ± 0.62
femur	2.84 ± 0.35	2.31 ± 0.68
brain	6.03 ± 0.80	3.95 ± 1.45
thymus	9.04 ± 1.54	7.00 ± 0.94
interscapular BAT	5.52 ± 1.80	24.31 ± 10.03
inguinal WAT	1.63 ± 0.50	5.66 ± 2.36

C



D

organs \ group	[123I]mIBG %ID/g Control	CL316,243
blood	0.69 ± 0.47	0.31 ± 0.13
heart	15.36 ± 3.48	14.24 ± 3.31
liver	7.57 ± 1.73	8.37 ± 1.25
lungs	7.46 ± 2.42	6.87 ± 1.69
thyroid	5.37 ± 2.34	7.04 ± 1.74
spleen	5.19 ± 1.54	7.91 ± 1.74
kidneys	2.53 ± 0.62	3.44 ± 1.18
stomach	4.64 ± 1.34	6.25 ± 0.82
small intestine	7.67 ± 1.94	7.91 ± 1.77
large intestine	3.10 ± 0.88	4.38 ± 0.68
testis	0.27 ± 0.07	0.42 ± 0.07
pancreas	3.11 ± 1.89	5.30 ± 1.02
muscle	0.50 ± 0.18	1.38 ± 0.44
femur	1.14 ± 0.29	1.69 ± 0.09
brain	0.14 ± 0.04	0.20 ± 0.03
thymus	1.89 ± 0.88	3.74 ± 0.70
interscapular BAT	1.01 ± 0.35	14.21 ± 3.70
inguinal WAT	0.53 ± 0.13	3.32 ± 0.53

Figure 3

Ex vivo biodistribution and quantitative analysis of [^{18}F]FDG uptake in control and CL316,243 treated mice. (A) *Ex vivo* biodistribution of [^{18}F]FDG at 1 h following [^{18}F]FDG injection in control and CL316,243 treated mice. (B) Quantitative analysis of [^{18}F]FDG uptake in various organs. [^{18}F]FDG uptake in each organ was normalized to organ weight and expressed as the percentage of injected dose per gram

(%ID/g). (C) *Ex vivo* biodistribution of [^{123}I]mIBG at 1 h following [^{123}I]mIBG injection in control and CL316,243 treated mice. (D) Quantitative analysis of [^{123}I]mIBG uptake in various organs. [^{123}I]mIBG uptake in each organ was normalized to organ weight and expressed as the percentage of injected dose per gram (%ID/g). Data are presented as mean ± SD. Data is presented as mean ± SD. * $p < 0.05$, compared with the control and CL316,243 treated groups.

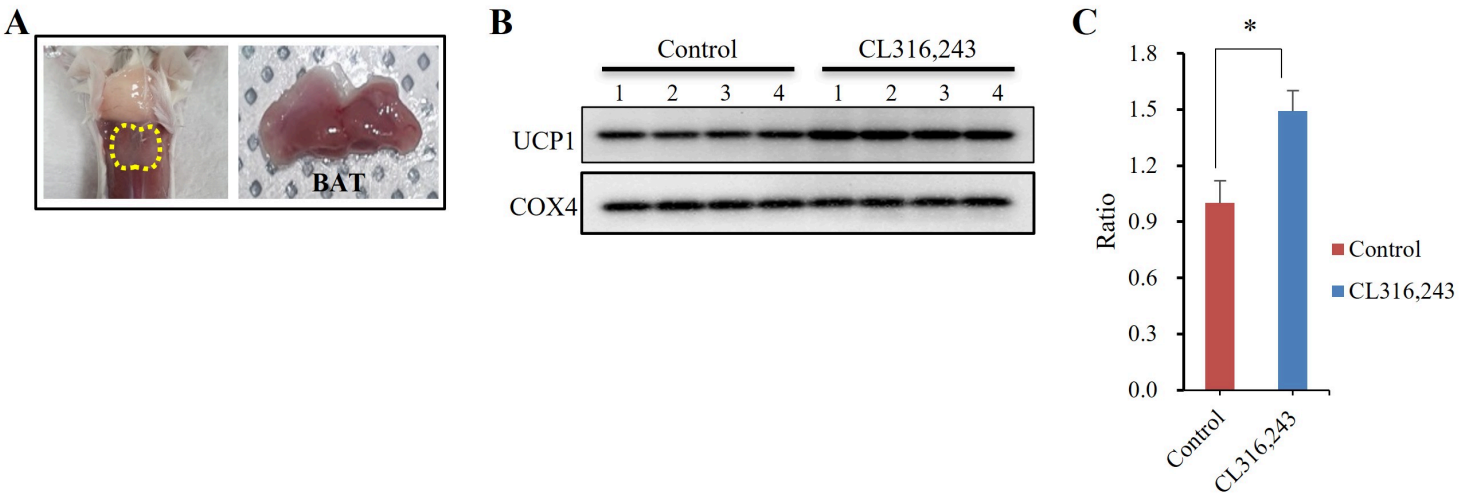


Figure 4

Quantitative measurement of UCP1 expression in BAT. (A) Representative images of interscapular BAT (yellow dotted line) collected from mouse for Western blot. (B) UCP1 protein expression in interscapular BAT from control and CL316,243 treated groups were analyzed by Western blot. COX4 was used as loading control. (**C**) Bars are the ratio of band intensity of UCP1 relative to that of COX4. * $p < 0.05$,compared with the control and CL316,243 treated groups.

Supplementary Files

This is a list of supplementary files associated with this preprint. Click to download.

- Supplementaryinformationchoi.pdf